A EUROPEAN JOURNAL

CHEMPHYSCHEM

OF CHEMICAL PHYSICS AND PHYSICAL CHEMISTRY

Accepted Article

Title: Preservation of Nuclear Spin Order by Precipitation

Authors: James Eills, Javier Alonso-Valdesueiro, David Enrique Salazar Marcano, Jesse Ferreira da Silva, Shamim Alom, Gregory Jon Rees, John Vincent Hanna, Marina Carravetta, and Malcolm Harris Levitt

To be cited as: *ChemPhysChem* 10.1002/cphc.201701189

Link to VoR: http://dx.doi.org/10.1002/cphc.201701189

A Journal of

ChemPubSoc Europe

WILEY-VCH

www.chemphyschem.org

Preservation of Nuclear Spin Order by Precipitation

James Eills[1,*], Javier Alonso-Valdesueiro[1], David E. Salazar Marcano[1], Jesse Ferreira da Silva[1], Shamim Alom[1], Gregory J. Rees[2], John V. Hanna[2], Marina Carravetta[1], and Malcolm H. Levitt[1]

[1] *School of Chemistry, University of Southampton, Southampton, United Kingdom*
[2] *Department of Physics, University of Warwick, Coventry, United Kingdom*
[*] Corresponding author: eills@soton.ac.uk

Abstract

We demonstrate that non-equilibrium nuclear spin order survives precipitation from solution and redissolution. The effect is demonstrated on ^{13}C- and ^{2}H-labeled sodium fumarate, with precipitation and dissolution achieved by altering the pH. The lifetime of the spin magnetization in the precipitate suspension is found to be much longer than in solution. Our preliminary results show an extension of the effective T_1 for the metabolite fumarate by a factor of ∼6. We show that when the free radical agent TEMPO is present in the solution, it is not incorporated into the precipitate, suggesting that this procedure may provide a means to store and transport agents polarized by dynamic nuclear polarization. Although the relaxation time, T_1, of the precipitate suspension is longer than that of the same molecules in solution, it is significantly shorter than that observed in the immobilized solid state.

Keywords: NMR, Relaxation, Precipitation, Spin Diffusion

Nuclear magnetic resonance (NMR) provides valuable chemical, structural, and dynamical information, but suffers from low signal strength. Hyperpolarization can be used to enhance the nuclear spin order in molecules by factors of $\sim 10^5$ compared to high field thermal equilibrium magnetization, to give greatly enhanced signals [1, 2, 3, 4, 5, 6, 7, 8, 9, 10]. Clinical studies involving hyperpolarized [1-^{13}C]pyruvate have been used to monitor tumour metabolism [2]. In vivo imaging studies have also been performed using hyperpolarized [1-^{13}C]fumarate [3].

Hyperpolarization methods are limited by an intrinsic longitudinal relaxation time (T_1) that governs the return of non-equilibrium magnetization to thermal equilibrium. The time for extracting the sample from the hyperpolarization equipment, purification, transport, delivery, and signal acquisition is often similar to the nuclear T_1, meaning that the polarizer needs to be located close to the point of use.

Efforts have been made towards the goal of storing hyperpolarized magnetization in the solid state [11, 12]. This is difficult in the case of dynamic nuclear polarization (DNP) where radicals are used for the polarization step, because they can induce rapid nuclear spin relaxation, especially in the solid state [13]. One approach employs heterogeneous materials, in which the hyperpolarized spin order is transported by spin diffusion to regions distant from the unpaired electron sites [4]. Another approach is to induce radical formation at low temperature by ultraviolet irradiation. The UV-induced radicals are quenched when the sample is warmed [5]. It is also possible to immobilize the radicals by attachment to a matrix, so that they remain behind when the polarized material is flushed out [9, 10].

In this paper we demonstrate the possibility of a different procedure, in which a polarized solution is prepared and the sample precipitated to form a suspension of microcrystals. We show that non-equilibrium magnetization is substantially preserved in this process, allowing the polarized substance to be liberated into solution by redissolving the solid at a later time. This can extend the effective nuclear T_1 because, under our experimental conditions, the solid-state T_1 is significantly longer than the solution-state T_1. We also show that the free radicals in solution are effectively excluded from the solid precipitate.

A crucial aspect of this experiment is the nontrivial

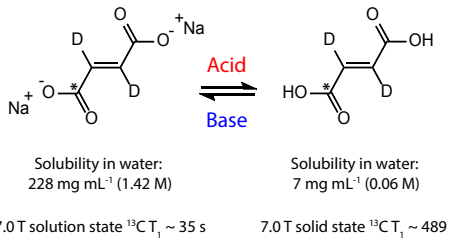

Figure 1: Solubility and relaxation properties of the labeled fumarate. The solution-state T_1 is for a 1.2 M sample at 298 K. The solid-state T_1 is for the 1-^{13}C site in a pure, dry sample at 298 K.

demonstration that nuclear spin polarization is not lost during the phase transitions. Other cases where spin magnetization is known to be preserved through phase transitions include dissolution-DNP [6, 7] and the freezing and sublimation of hyperpolarized ^{129}Xe gas [8] or molecules dissolved within [14, 15].

In this work, the precipitation and redissolution was carried out on a sample of disodium fumarate-1-^{13}C-2,3-d_2, mixed with disodium fumarate-2,3-d_2 in a 1:9 ratio, and dissolved in water. Disodium fumarate readily dissolves in water as sodium cations and the fumarate

dianion, while the protonated form, fumaric acid, is relatively insoluble (7 mg mL^{-1}) [16]. By altering the pH of the solution, we are able to precipitate and dissolve the fumarate at will (Figure 1).

The inversion recovery experiment shown in Figure 2a

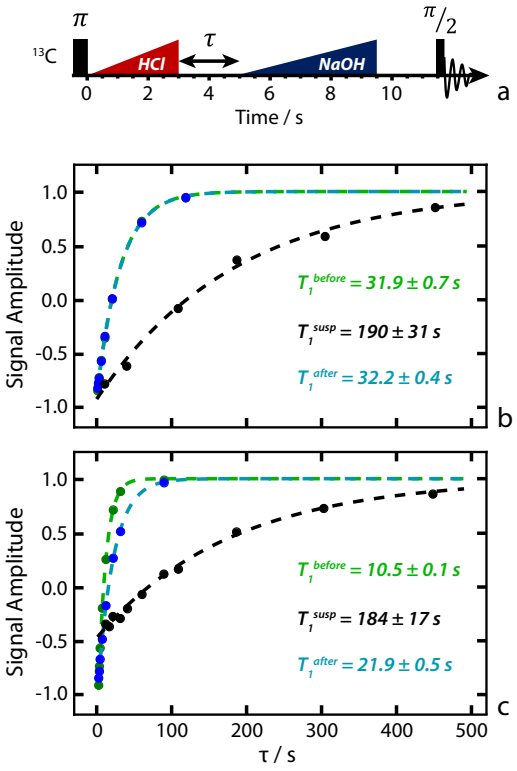

Figure 2: a) Inversion-recovery pulse sequence, including the acid and base additions. The addition of HCl causes fumaric acid to precipitate out of solution, and the addition of NaOH causes redissolution. b) A relaxation plot of the fumarate-1-^{13}C-2,3-d$_2$ carbonyl ^{13}C NMR signals. Black points correspond to the experiment in (a). Green and blue points are from a conventional solution-state inversion-recovery relaxation measurement on a 1.2 M sample at 298 K before and after the acid/base additions, respectively. Dashed lines are the monoexponential best-fit curve for each dataset. The three data sets have been normalized to recover to a signal amplitude of 1. c) A relaxation plot acquired in the same manner as that shown in (b), but with TEMPO radical present in the sample at an initial concentration of 2 mM.

was performed on six samples, using a different τ delay for each, and the results are shown in Figure 2b. The green and blue relaxation curves were acquired by performing experiments on a sample of 1.2 M sodium fumarate-1-^{13}C-2,3-d$_2$ in water before and after the acid/base addition, respectively. This data allows comparison with a sample that wasn't precipitated during the experiment, and relaxed with the solution-state T_1. Using the procedure in Figure 2a, an effective relaxation time for the microcrystalline suspension, T_1^{susp}, of 190±31 s was estimated, a factor of ~6 times longer than the solution-state T_1 of ~32 s. For each dataset, the signal was normalized and fit to an exponential of the form $1 - Ae^{-t/T_1}$, where A and T_1 are variables.

A comparison between the powder x-ray diffraction (PXRD) patterns for the precipitated particles and a stock sample of fumaric acid is shown in Figure 3. The sample preparation is given in the Methods. The sharp

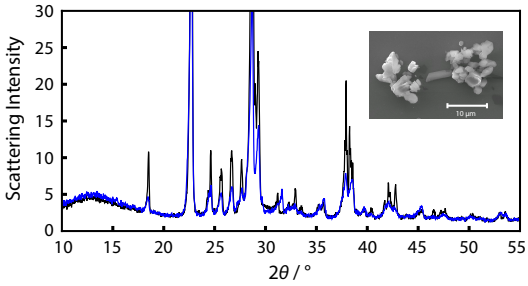

Figure 3: Powder x-ray diffraction scattering patterns for stock fumaric acid (black), and precipitated fumaric acid (blue). The scattering intensity has been normalized to 100 for the maximum scattering in stock fumaric acid in both spectra. An inset shows an SEM image of the precipitated fumaric acid.

peaks indicate the particles in both cases are largely crystalline, and the overlap between the patterns suggests the crystal structures are nearly identical. There appears to be a small degree of amorphicity, as indicated by the broad feature centered at $2\theta = 14°$. Importantly, this feature is of equal intensity for the precipitate and stock fumaric acid.

A scanning electron microscopy (SEM) image is shown in the inset of Figure 3. From this we estimate an average particle diameter of approximately 1 μm, but the variance is clearly large.

The field-dependence of the ^{13}C T_1 was measured in the solid state on samples of dry fumaric acid-1-^{13}C-2,3-d$_2$ and fumaric acid-2,3-d$_2$ in a 1:9 ratio. The samples were mixed polycrystalline solids and the T_1 was measured by saturation recovery, and the results are shown in Figure 4. The decrease in relaxation time with increasing field suggests that the dominant relaxation mechanism involves the chemical shift anisotropy.

Solid-state relaxation measurements were also performed on the precipitated samples of fumarate-1-^{13}C-2,3-d$_2$ (10% ^{13}C labeling), both before and after drying the precipitate (see Methods). The solid-state T_1 measured at 7.0 T under magic angle spinning (MAS) was 477±44 s for the wet precipitate, and 489±26 s for the dry precipitate. These are the same within the margins of error, and both are a factor of ~2.5 times longer than T_1^{susp}.

One possible reason for this discrepancy is that the temperature of the suspended particles is significantly raised by the chemical reaction in solution. The temperature of the sample was measured throughout the precipitation procedure, and showed a significant increase immediately after the acid and base additions, but never exceeded 38°C. The solid-state T_1 for the wet precipitate sample was measured to be 572±62 s at 7.0 T under MAS at 35°C. Since this is larger than that of the wet precipitate (477±44 s) measured at room temperature (~23°C), a local increase in temperature upon precipitation is unlikely to explain the discrepancy.

At this point we do not understand the different relaxation behaviour of the suspended particles and the solid precipitate. One possibility is that amorphous or surface regions of the suspended microcrystals act as relaxation sinks which are brought into contact with the bulk through ^{13}C-^{13}C spin diffusion, driven by the

slow tumbling motion of the suspended particles, as in rotational resonance phenomena [17, 18]. This mechanism requires dipole-dipole coupling between nearby ^{13}C nuclei, and would be effectively suppressed in the MAS relaxation experiments. Another possibility is that crystallite molecules are in exchange with the surrounding solution, so that the relaxation rate constant corresponds to a weighted average of the solid and liquid values. However, this mechanism appears to be inconsistent with observations for the wet precipitate, for which the ^{13}C relaxation time is much longer than in the particle suspension and is indistinguishable from that of the dry solid (see above). We are not aware of prior studies of nuclear spin-relaxation in particle suspensions. This provides an intriguing direction for further study.

The effect of including TEMPO ((2,2,6,6-tetramethylpiperidin-1-yl)oxyl) radicals at a concentration of 2 mM in the solution was investigated. The radicals are paramagnetic and can provide an efficient source of nuclear spin relaxation, especially in the solid state. For the precipitation measurements, shown in Figure 2c, the same experimental procedure was used as before. A T_1^{susp} of 184±17 s was measured, compared to solution-state T_1 values of 10.5 and 22 s before and after addition of the acid and base, respectively. The slower ^{13}C relaxation in solution after the acid and base additions is attributed to the dilution of the radicals by the additional liquids.

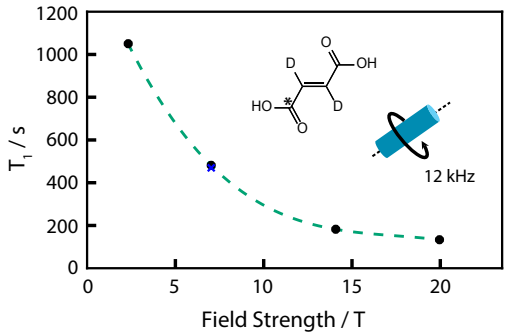

Figure 4: The T_1 of the carbonyl ^{13}C in dry fumaric acid-1-^{13}C-2,3-d_2 (black points) as a function of static field strength. Measurements were performed on samples packed into 4 mm zirconia rotors under 12 kHz MAS. The dashed line is an interpolation to guide the eye. The T_1 of a wet sample of fumaric acid-1-^{13}C-2,3-d_2 is shown by the blue cross. Within the error, the solid-state T_1 at 7.0 T is the same for a wet or dry sample.

The solution-state T_1 values are shorter in the presence of radicals, and strongly depend on the TEMPO concentration [19, 20]. However, within experimental error, the measured T_1^{susp} values of the particle suspension are the same with and without radicals.

Electron paramagnetic resonance (EPR) measurements were performed to quantify the concentration of TEMPO contamination in the precipitated crystals (Figure 5). Additional spectra were taken of 10 μM TEMPO and 1.2 M sodium fumarate in water. TEMPO radicals in solution produce a characteristic three line EPR profile from the electron hyperfine coupling to the spin-1 nitrogen-14 nucleus [21]. After correcting for the

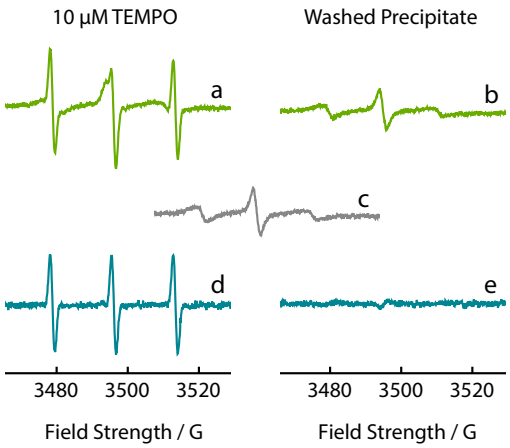

Figure 5: A comparison of solution-state EPR spectra for a co-solution of 1.2 M sodium fumarate and 10 μM TEMPO in water, and the precipitate from our experiment. The precipitate solution was prepared as described in the Methods. a) Spectrum of 1.2 M sodium fumarate and 10 μM TEMPO solution. b) Spectrum after precipitation of a 1.2 M sodium fumarate and 2 mM TEMPO solution, washing, and dissolving in NaOH solution. c) The background signal of pure sodium fumarate solution. d) Residual spectrum after subtracting the background signal from (a). e) Residual spectrum after subtracting the background signal from (b).

background signal from metal impurities in the fumarate solution, this pattern was observed in the 10 μM TEMPO solution, but not in the solution of washed precipitate. An upper bound on the radical concentration was set at 1 μM as this was the detection limit.

These results show that to a good approximation the radical molecules are excluded from the precipitate, suggesting that the precipitation step acts as an effective purification method for removing contaminants from the hyperpolarized substance.

We have demonstrated that by precipitating the metabolite fumarate out of solution, non-equilibrium nuclear spin order can persist for times much longer than the solution-state T_1. We also demonstrate the precipitation step can purify the sample of undesired contaminants, such as free radicals, which are often used in dissolution DNP experiments. This technique may therefore be useful for preserving substances in a state of non-equilibrium nuclear spin order, as generated by hyperpolarization techniques such as dynamic nuclear polarization. For the current case of isotopically enriched fumarate, the relaxation times observed in the solid state are found to be considerably longer at low magnetic field, which holds promise for the low-field transport of hyperpolarized substances from the point of polarization to the point of use. Although this method is likely to be limited in scope to substances with suitable physicochemical characteristics, some suitable cases do exist and are known to be important. Hyperpolarized fumarate is already used for investigations of cancer [3]. We are now planning trial experiments in which hyperpolarized fumarate solutions are precipitated by the method above.

Methods

Precipitation experiments

All precipitation experiments were performed with 1.2 M samples of disodium fumarate-1-^{13}C-2,3-d_2, mixed with disodium fumarate-2,3-d_2 in a 1:9 ratio, and dissolved in 1 mL of water, and loaded into 10 mm NMR tubes. Deuteration was used to extend the solution-state carbonyl ^{13}C T_1. The experiments were performed at a magnetic field of 7.0 T (300 MHz ^{1}H frequency) using a Bruker Avance III spectrometer. The experimental apparatus is shown in Figure 6.

The precipitation and redissolution steps were performed separately using 0.22 mL 12 M HCl and 0.33 mL 9 M NaOH. These two solutions were loaded into separate 1/16 inch PTFE (polytetrafluoroethylene) tubes which terminated just below the surface of the sample. The 1 mL sodium fumarate sample was placed inside the probe's radiofrequency (RF) coil, with the PTFE tubes penetrating by ∼5 mm. The small initial sample volume ensures that all ^{13}C spins experience a strong radiofrequency field (see below).

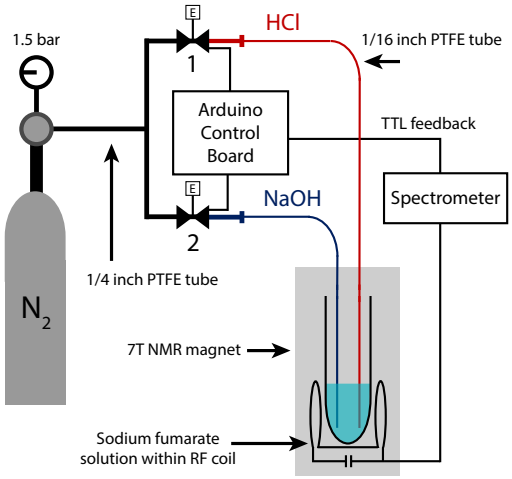

Figure 6: Sketch of the apparatus. The acid and base were loaded individually in 1/16 inch PTFE tubes, which were placed in a 10 mm NMR tube in the spectrometer. The N_2 flow to inject acid/base was controlled by opening the electrovalves, interfaced with the spectrometer through an Arduino board.

The NMR experiments in Figure 2 were performed using inversion recovery sequences, with precipitation by addition of acid, and dissolution by addition of base, during the variable wait time. A π pulse was applied to invert all carbon spins, followed by a delay of 0.1 s. The HCl solution was added over 3 s by flowing N_2 gas at a pressure of 1.5 bar from behind, and fumaric acid precipitated out of the solution. After a variable delay τ, the NaOH solution was injected over 4.5 s, followed by a 2 s wait time for the solution to settle, and the signal acquired with a $\pi/2$ pulse.

The small initial sample volume (1 mL) was to ensure that the sample was contained entirely within the RF coil, to ensure that the π pulse inverted the ^{13}C magnetization of the entire sample, to a good approximation. This avoids problems associated with the physical mixing of sample regions, some of which contain ^{13}C nuclei that experienced a near-ideal π pulse, and some of which were only partially affected.

Adding the acid and base increased the sample volume by 55%, introduced a high concentration of ions, increased the temperature by 17 K and altered the shims. The introduction of ions reduced the total RF power that perturbed the nuclei, but in a reproducible manner between experiments, so we were able to calibrate the final $(\pi/2)_y$ pulse length accordingly. The shim and temperature alteration was ignored, because the peak integrals should be independent of this.

Sample characterisation

To prepare the precipitated solid for PXRD and SEM characterisation, 2.2 mL 12 M HCl was added to 10 mL 1.2 M sodium fumarate. The resulting solid suspension was filtered and dried under vacuum for 2 h. The stock fumaric acid used for PXRD comparison was purchased from Sigma Aldrich and used directly.

For the PXRD experiments, the x-ray source was swept from 5° to 80° (2θ) over 200 s. Cu Kα x-rays at a wavelength of 1.54 Å were used.

Solid-state T_1 measurements

Solid-state relaxation experiments at fields of 2.3, 7.0, 14.1 and 20.0 T were performed on a dry sample of fumaric acid-1-^{13}C-2,3-d_2 and fumaric acid-2,3-d_2 (mixed polycrystalline solids) in a 1:9 ratio, under 12 kHz MAS packed in a 4 mm zirconia rotor. Saturation recovery pulse sequences were used to measure the T_1 without an initial ^{1}H-^{13}C cross polarization step.

Solid-state relaxation measurements were also performed at a field strength of 7.0 T on a wet precipitated sample of fumaric acid-1-^{13}C-2,3-d_2 and fumaric acid-2,3-d_2 in a 1:9 ratio, to mimic the solid formed in the precipitation experiments. 5 mL of 12 M HCl was added to a 5 mL sample of 1.2 M sodium fumarate-1-^{13}C-2,3-d_2 (10% ^{13}C labeling) in water. The resulting precipitate was partially dried with filter paper and this wet solid was packed into a 4 mm zirconia rotor. A saturation recovery sequence was used to measure the T_1 under 12 kHz MAS.

EPR measurements

To a solution of 1.2 M sodium fumarate and 2 mM TEMPO in water, HCl was added to precipitate out fumaric acid. The crystals were washed with 25 mL water to remove residual TEMPO from the crystal surfaces, and dried by filtering off the water using a Hirsch funnel. Fumaric acid crystals (139 mg) were redissolved with 1 mL 2.4 M sodium hydroxide in water. Solution-state EPR measurements were taken using an EMX Micro EPR spectrometer with 16 scans of 100 G sweep width lasting 10 s each. The microwave frequency was 9.82 GHz

at a power of 6 mW.

Acknowledgements

This research was supported by EPSRC (UK) (grant numbers EP/P009980 and EP/M508147/1) and Bruker BioSpin. The UK 850 MHz High Field NMR Facility and the lower field instruments in Millburn House used in this research were funded by EPSRC, BBSRC, the University of Warwick and the Birmingham Science City Advanced Materials Projects 1 and 2, the latter source being supported by Advantage West Midlands and the European Regional Development Fund. We acknowledge Stuart Elliott for help with EPR measurements, and India Willimott for help with SEM and PXRD experiments.

References

[1] G. Jeschke, L. Frydman, *J. Magn. Reson.* **2016**, *264*, 1–2.

[2] S. J. Nelson, J. Kurhanewicz, D. B. Vigneron, P. E. Z. Larson, A. L. Harzstark, M. Ferrone, M. van Criekinge, J. W. Chang, R. Bok, I. Park *et al.*, *Sci. Transl. Med.* **2013**, *5*, 198ra108–198ra108.

[3] M. R. Clatworthy, M. I. Kettunen, D. E. Hu, R. J. Mathews, T. H. Witney, B. W. C. Kennedy, S. E. Bohndiek, F. A. Gallagher, L. B. Jarvis, K. G. C. Smith, K. M. Brindle, *P. Natl. Acad. Sci.* **2012**, *109*, 13374–13379.

[4] X. Ji, A. Bornet, B. Vuichoud, J. Milani, D. Gajan, A. J. Rossini, L. Emsley, G. Bodenhausen, S. Jannin, *Nat. Commun.* **2017**, *8*, 13975.

[5] A. Capozzi, T. Cheng, G. Boero, C. Roussel, A. Comment, *Nat. Commun.* **2017**, *8*, year.

[6] J. H. Ardenkjær-Larsen, B. Fridlund, A. Gram, G. Hansson, L. Hansson, M. H. Lerche, R. Servin, M. Thaning, K. Golman, *Proc. Natl. Acad. Sci.* **2003**, *100*, 10158–10163.

[7] A. Bornet, R. Melzi, A. J. Perez Linde, P. Hautle, B. van den Brandt, S. Jannin, G. Bodenhausen, *J. Phys. Chem. Lett.* **2012**, *4*, 111–114.

[8] F. W. Hersman, I. C. Ruset, S. Ketel, I. Muradian, S. D. Covrig, J. Distelbrink, W. Porter, D. Watt, J. Ketel, J. Brackett *et al.*, *Acad. Radiol.* **2008**, *15*, 683–692.

[9] D. Gajan, A. Bornet, B. Vuichoud, J. Milani, R. Melzi, H. A. van Kalkeren, L. Veyre, C. Thieuleux, M. P. Conley, W. R. Grüning, M. Schwarzwälder, A. Lesage, C. Copéret, G. Bodenhausen, L. Emsley, S. Jannin, *Proc. Natl. Acad. Sci.* **2014**, *111*, 14693–14697.

[10] B. Vuichoud, A. Bornet, F. De Nanteuil, J. Milani, E. Canet, X. Ji, P. Miéville, E. Weber, D. Kurzbach, A. Flamm, et al., *Chem. Eur. J.* **2016**, *22*, 14696–14700.

[11] M. Gatzke, G. D. Cates, B. Driehuys, D. Fox, W. Happer, B. Saam, *Phys. Rev. Lett.* **1993**, *70*, 690–693.

[12] H.-U. Kauczor, R. Surkau, T. Roberts, *Eur. Radiol.* **1998**, *8*, 820–827.

[13] W. E. Blumberg, *Phys. Rev.* **1960**, *119*, 79.

[14] N. Lisitza, I. Muradian, E. Frederick, S. Patz, H. Hatabu, E. Y. Chekmenev, *J. Chem. Phys.* **2009**, *131*, 044508.

[15] A. Cherubini, G. S. Payne, M. O. Leach, A. Bifone, *Chem. Phys. Lett.* **2003**, *371*, 640–644.

[16] S. H. Yalkowsky, Y. He, P. Jain, *Handbook of aqueous solubility data*, CRC press, **2016**.

[17] M. G. Colombo, B. H. Meier, R. R. Ernst, *Chem. Phys. Lett.* **1988**, *146*, 189–196.

[18] M. H. Levitt, D. P. Raleigh, F. Creuzet, R. G. Griffin, *J. Chem. Phys.* **1990**, *92*, 6347–6364.

[19] J. Kowalewski, L. Maler, *Nuclear spin relaxation in liquids: theory, experiments, and applications*, CRC press, **2006**.

[20] P. Vallet, Y. Van Haverbeke, P. A. Bonnet, G. Subra, J.-P. Chapat, R. N. Muller, *Magn. Reson. Med.* **1994**, *32*, 11–15.

[21] A. Schweiger, G. Jeschke, *Principles of Pulse Electron Paramagnetic Resonance*, Oxford University Press, **2001**.